NRC Research Press

ARTICLE

Landslide hazard assessment using digital elevation models

Gordon A. Fenton, Amanda McLean, Farrokh Nadim, and D.V. Griffiths

Abstract: Human beings are, in general, risk-averse and willing to go to great lengths to reduce failure consequences. However, if the underlying issues are not understood, effective action cannot properly be taken. A landslide hazard assessment framework capable of estimating regional probabilities of slope failure can be used to aid a vast number of communities currently living in landslide "danger zones". Such a framework would provide a tool with which community resources can be optimized and ensure that appropriate preparedness and mitigation strategies are in place. Maximum slope angles, as estimated using digital elevation models (DEMs), are one of the most important indicators for landslide hazard assessment. This paper uses local averaging theory to determine how the resolution of DEMs affects regional landslide probability estimates. Emphasis is on a regional landslide hazard assessment, measured by the probability that one or more slopes of at least a critical minimum scale will fail within the region.

Key words: regional landslide hazard assessment, digital elevation models (DEM), slope failure probability, slope stability, random finite element method (RFEM).

Résumé : Les humains tentent généralement d'éviter les risques et sont prêts à prendre les actions nécessaires pour réduire les conséquences des ruptures. Cependant, si les causes ne sont pas comprises, des actions efficaces ne peuvent pas être appliquées. Un cadre d'évaluation du risque de glissement de terrain capable d'estimer les probabilités régionales d'une rupture de pente peut être utile à un grand nombre de communautés qui vivent présentement dans des « zones de danger » de glissement de terrain. Un tel cadre permettra d'offrir un outil avec lequel les ressources des communautés pourront être optimisées et qui s'assurera d'une prévention adéquate et que les stratégies d'atténuation sont en place. Les angles maximaux des pentes, tels qu'estimés à l'aide de modèles digitaux d'élévation (MDE), sont parmi les indicateurs les plus importants pour l'évaluation des risques de glissement de terrain. Cet article se base sur la théorie des moyennes locales pour déterminer comment la résolution des MDE affecte les estimations des probabilités de glissement de terrain à l'échelle régionale. L'emphase est placée sur une évaluation du risque régional de glissement de terrain, mesuré par la probabilité qu'une ou plusieurs pentes d'au moins une échelle critique minimum cèdent dans la région. [Traduit par la Rédaction]

Mots-clés : évaluation régionale du risque de glissement de terrain, modèle digital d'élévation (MDE), probabilité de rupture de pente, stabilité de pente, méthode par éléments finis aléatoire (RFEM).

Introduction

Landslides are a common and devastating type of natural disaster, often causing loss of life and irreparable damage. Given the unstable nature of the natural environment, particularly after humans have modified it, these geohazards are increasing in frequency in many regions around the globe (Nadim et al. 2006). Thus, there is a pressing need to improve techniques for landslide risk management.

Landslide risk refers to the probability that a region will undergo significant levels of damage from a landslide event — the risk is a function of both hazard and vulnerability (UNDRO 1979; Nadim et al. 2006). This study focuses on landslide *hazard* assessment, where a hazard is defined as a slope failure leading to negative human consequences. The hazard level is defined herein as the probability that at least one slope, of sufficient size to lead to negative human consequences, fails within the region under consideration. The hazard level thus ranges from 0 (not possible) to 1 (certain). It is recognized that the time span considered is also intimately related to the assessed hazard level. For example, for a given region, the landslide hazard level over a single day might be quite low but may become quite high if the time span is increased to thousands of years. This paper does not directly consider the time dependence of landslide risk — the time dependence shows up in the parameters of the ground properties used to model the slopes in the region. In other words, as the timespan considered increases, the variability of the ground parameters also increases (and (or) the mean strength decreases). The nature of this increase (decrease) is still very poorly understood and is beyond the scope of this paper. It is assumed here that the users of this framework will have some idea of the variability of the ground properties over the timespan of interest within the region under study.

Digital elevation models (DEM) are effective tools for estimating slope instability levels because they can be used to predict the regional distribution of maximum slope angles. Because the equilibrium state of any terrain is a flat plane, the further a given terrain is from a flat plane (i.e., the steeper the slope), the more likely the terrain is to fail to achieve its equilibrium state. DEMs use remote sensing techniques to measure surface elevations over a series of adjacent areal domains (*cells*) and the data are stored in a grid of cells. The maximum slope angle can then be evaluated for each cell using the average surface elevations provided for that

Received 27 September 2011. Accepted 13 March 2013.

G.A. Fenton. Faculty of Civil Engineering and Geosciences, Delft University of Technology, Delft, the Netherlands; Department of Engineering Mathematics, Dalhousie University, Halifax, NS, Canada.
A. McLean. Department of Engineering Mathematics, Dalhousie University, Halifax, NS, Canada.
F. Nadim. Norwegian Geotechnical Institute, Oslo, Norway.
D.V. Griffiths. Division of Engineering, Colorado School of Mines, Golden, CO, USA.
Corresponding author: Gordon A. Fenton (e-mail: Gordon.Fenton@dal.ca).

cell in relation to its neighbouring cells. Many algorithms have been implemented in the past to estimate maximum slope angles from DEMs. For instance, Jones (1998) and Raaflaub and Collins (2006) each identified and compared eight different DEM slope calculation algorithms. This paper uses a second-order finite-difference (i.e., using two points in each coordinate direction) algorithm to estimate maximum slope angles. Note that although higher order approximations are available, the higher order polynomials employed result in an artificial increase in the slope variance, which is undesirable.

Maximum slope angles derived from DEMs are referred to as *perceived* maximum slope angles in this paper because their values are dependent upon the resolution of the DEM. The DEM resolution introduces a scale issue because the DEM is averaging the actual terrain over each DEM cell — the larger the DEM cell, the greater the resulting terrain smoothing. Because smoothing damps out the more frequent short steep slopes in favour of the "average" longer and shallower slopes, maximum slope angles derived from low resolution models will be underestimated. Maximum slope angles, as perceived by multiple DEM resolutions, were examined by Chang and Tsai (1991) with cells ranging from 8 to 80 m in size, by Claessens et al. (2005) with cells from 10 to 100 m, by Deng et al. (2007) with cells from 5 to 480 m, and by Chow and Hodgson (2009), on microscale terrain, with 2 to 10 m cell dimensions. The results of each of these experiments indicated that higher resolution models map more terrain variance and steeper mean maximum slope angles than low resolution models. However, while many of these papers allude to the impact of DEM resolution on perceived maximum slope angles, they do not present a theoretical way of quantifying this effect. This paper provides such a way.

Nadim et al. (2006) examined this scaling issue in more depth in their study on landslide and avalanche hot spots. In their study, Nadim et al. used two DEM resolutions to estimate slope angles through multiple test regions (see also Jaedicke et al. 2010); a lower resolution DEM was used above 60 °N latitude and a higher resolution DEM was used below 60 °N latitude. In an attempt to overcome the inconsistencies between the slope angles perceived by each of these DEMs, Nadim et al. (2006) developed an approximate relationship between the DEM resolution (i.e., cell size) and the resulting perceived slope angles. For example, areas with slope angles estimated to be between 8° and 10° using the lower resolution (larger cell) DEM were assigned the same hazard class as were areas having slope angles between 12° and 18° according to the higher resolution (smaller cell) DEM. Nadim et al. thus provide an empirical approach to relating slope failure risk to DEM resolution. However, a more accurate theoretical-based calibration technique would greatly improve their model, which is the goal of this paper.

Zhang et al. (1999) also derived a relationship between DEM resolution and perceived maximum slope angles. They approached this issue using a variogram technique, based on the assumption that topography is, in general, fractal in nature (Peitgen and Saupe 1988). Unfortunately, the fractal model tended to break down in regions where the elevation changed rapidly and their results suggested that for low resolution DEMs the fractal scaling could significantly underestimate the regional probability of slope failure in regions with rapidly changing terrain — which are just the conditions that typically lead to high landslide risk.

In summary, it appears that little progress has been made towards producing a landslide hazard assessment model that overcomes the scaling issues associated with variable resolution DEMs. This paper thus concentrates on the development of a model that employs random field local averaging theory to evaluate regional landslide hazard levels at any resolution scale. The remainder of the paper is basically divided into two parts; (*i*) a proposed theoretical random field model, and (*ii*) an example case study to illustrate how the theoretical model is used to estimate regional landslide hazard levels.

The proposed theoretical model, described in the next three sections of the paper, combines the regional distribution of maximum slope angles (next section) with conditional slope failure probabilities (following section) to obtain estimates of the regional landslide hazard assessment (the subsequent section), which is the overall goal of this paper. Other issues, such as probabilities associated with landslide magnitude, are also discussed for completeness.

The second part of the paper, appearing in the "Case study" section, illustrates how the proposed theoretical model should be applied to a particular region to assess its regional landslide hazard. While the case study is based on a specific region near Chamonix, France, with real DEM data, the case study is not based on real geotechnical ground parameters obtained from a regional geotechnical investigation. This means that the case study results presented here should not be considered an actual landslide hazard assessment for the case study region. In practice, the methodology presented in this paper should combine DEM datasets with regional geotechnical investigations (or relevant engineering experience) to obtain a reasonable regional landslide hazard level estimate. More details, along with a second case study and further extensions to landslide vulnerability assessments, can be found in McLean (2011).

Distribution of maximum slope angle

The elevation measured over a cell within a DEM approximately represents the average elevation over the entire cell as perceived by the satellite or airplane composing the DEM. If the DEM cell is 100 m × 100 m in size, then elevation variations within this domain having scale less than 100 m will be smoothed over. In other words, small slopes (e.g., of extent 10 m) will not be resolved by this DEM even if the slope is extremely steep. Smaller DEM cells result in an increase in the amount of data available to describe the detailed topography of the terrain and thus the true slope distribution.

As resolution increases, slope variability also increases. If the natural terrain is studied at the microscale (e.g., at a scale much less than 1 m), a very wide range in slopes will be observed and many small-scale slope failures occur on a regular basis. Most of these small-scale slope failures are of no interest, because they do not result in observable or significant damage. In other words, failure of a 1 m slope is of little concern, while failure of a 1000 m slope is probably of significant concern. In general, there will be a critical slope dimension that is at the lower bound of concern, and this slope dimension will be referred to here as the "critical scale". The magnitude of the critical scale is selected by estimating the minimum scale at which a single slope failure would be deemed hazardous. As suggested earlier, the critical scale probably lies somewhere between 1 and 1000 m.

Using local averaging theory, a relationship can be derived between the DEM resolution and the perceived maximum slope angle distribution, making it possible to predict the distribution of maximum slope angles as perceived at any DEM resolution. This study is primarily concerned with landslide hazard analysis at the critical scale and above.

In the following the critical scale will be assumed to be 10 m, based purely on engineering judgement. In this section, the theory relating DEM resolution to maximum slope angle distribution is presented, and this theory is then used to establish the maximum slope angle distribution at the critical scale. In turn, the critical scale slope angle distribution can then be used to estimate the regional landslide hazard level (see the "Regional landslide hazard assessment" section).

Assuming that the average elevation over each DEM cell, having plan area $T_x \times T_y$, is taken at the center of the cell (x_T, y_T) and that

average elevations are recorded at regular intervals separated by distance T_x and T_y in each coordinate direction, a DEM produces a regular grid of adjacent locally averaged elevations, $Z_T(x_T, y_T)$. Furthermore, if $Z(x, y)$ is the actual surface elevation at surface location (x, y), where x and y are coordinate axes that are assumed to be aligned with the edges of the DEM and lie in the plane of the surface, then the local average elevation, $Z_T(x_T, y_T)$ over a domain of size $T_x \times T_y$ is given by

$$(1) \qquad Z_T(x_T, y_T) = \frac{1}{T_x T_y} \int_{y_T - T_y/2}^{y_T + T_y/2} \int_{x_T - T_x/2}^{x_T + T_x/2} Z(s, r)\, ds\, dr$$

Based on the grid of locally averaged elevations provided by a DEM, a grid of perceived slope angles, S_{T_x} and S_{T_y}, can be estimated in each of the two coordinate directions, x and y, using the following second-order finite-difference approximations,

$$(2a) \qquad S_{T_x}(x_T, y_T) = \frac{Z_T(x_T + T_x, y_T) - Z_T(x_T - T_x, y_T)}{2T_x}$$

$$(2b) \qquad S_{T_y}(x_T, y_T) = \frac{Z_T(x_T, y_T + T_y) - Z_T(x_T, y_T - T_y)}{2T_y}$$

where the averaging cell dimension is assumed to be $T_x \times T_y$. These equations must be modified for the cells along the edge of the DEM. For example, $S_{T_x}(x_T, y_T) = [Z_T(x_T, y_T) - Z_T(x_T - T_x, y_T)]/T_x$ along the right edge of the region.

If it is assumed that each DEM cell represents a plane whose center, (x_T, y_T), is at its average elevation, $Z_T(x_T, y_T)$, then the *perceived maximum* slope angle of each cell can be estimated by using simple geometry. Given the directional derivatives of eq. (2), the maximum slope of the resulting plane is given by

$$(3) \qquad S_{T_m}(x_T, y_T) = \sqrt{S_{T_x}^2(x_T, y_T) + S_{T_y}^2(x_T, y_T)}$$

It is assumed that landslides will occur in the direction having maximum slope angle given by eq. (3). This is referred to as a *perceived* maximum slope angle because the true slope is approximated by locally averaged DEM measurements.

The distribution of the perceived maximum slope angles, S_{T_m}, throughout a domain will follow a Rayleigh distribution if the following conditions are met:

1. The slope angles (eq. (2)) in the x and y directions are independent and identically normally distributed. This will generally hold if the underlying elevation data are normally distributed and the DEM cells are square ($T_x = T_y$).
2. The slope angles in the x and y directions have zero means (i.e., the average ground surface over the entire region considered is flat).

It will be shown below that these conditions are approximately met for the test region considered later in this paper, except for the requirement that the DEM cells be square (because the test region is well away from the equator). The cumulative distribution function of the Rayleigh distribution is given by

$$(4) \qquad F_s(s) = P[S \le s] = 1 - \exp\left(-\frac{s^2}{2\sigma_{S_T}^2}\right)$$

where σ_{S_T} is the standard deviation of the perceived slope angles.

For numerical purposes, it is convenient to discretize the slope angles into a sequence of disjoint ranges of the form

$$(5) \qquad s_i = [s_{i-}, s_{i+})$$

where

$$(6a) \qquad s_{i-} = \tan\left(d_i - \frac{\Delta d}{2}\right)$$

$$(6b) \qquad s_{i+} = \tan\left(d_i + \frac{\Delta d}{2}\right)$$

and $d_i = i\Delta d$ is the slope angle in degrees. In this paper Δd is taken to be 1° and eq. (6) is used to define s_{i-} and s_{i+} for $i = 1, \ldots, 89$. For $i = 0$, only the positive half of the range is considered;

$$(7) \qquad s_0 = \left[0, \tan\left(\frac{\Delta d}{2}\right)\right)$$

so that $s_{0-} = 0$ and $s_{0+} = \tan(\Delta d/2)$. Vertical slopes, where $d_i = 90°$, have been excluded from consideration because they cannot be resolved by the DEM nor under local averaging (which is also true of negative "overhanging" slopes). Thus, the sequence of slope ranges starts from $s_{min} = s_0$ and increase up to $s_{max} = s_{89}$. Alternative discretization schemes can easily be considered simply by changing the value of Δd and the upper bound on i in the preceding equations.

Hereinafter, the event $(S = s_i)$ will be taken to mean that the random slope angle, S, is an element of the range s_i, (i.e., that $s_{i-} \le S < s_{i+}$). In some cases, s_i is referred to as being a single slope angle, rather than a range — for example, when the failure probability of a slope with a given slope angle is being evaluated. In this case, s_i is to be interpreted as being at the midpoint of its range (i.e., $s_i = \tan(d_i)$), and it is assumed that the slope failure probability remains constant over the actual range of s_i. As long as Δd is kept relatively small (e.g., 1°), this assumption will be reasonably valid.

Based on eqs. (4)–(7), the distribution of maximum slope angles can be estimated as follows for $i = 0, 1, \ldots, 89$;

$$(8) \qquad P[S_{T_m} = s_i] = P[s_{i-} \le S_{T_m} < s_{i+}] = F_S(s_{i+}) - F_S(s_{i-}) = \exp\left(-\frac{s_{i-}^2}{2\sigma_{S_T}^2}\right) - \exp\left(-\frac{s_{i+}^2}{2\sigma_{S_T}^2}\right)$$

To evaluate eq. (8), the standard deviation of the slope angles, σ_{S_T}, must be determined.

Stationarity, or statistical homogeneity, of $Z(x, y)$ implies that its mean, variance, and correlation structure are independent of position. In other words, the mean and variance are constant over space and the correlation structure depends only on relative positions. In this research, stationarity has been assumed and under this condition both $S_{T_x}(x, y)$ and $S_{T_y}(x, y)$ have zero mean and the following variance (Fenton and Griffiths 2008):

$$(9) \qquad \mathrm{Var}[S_{T_x}] = \frac{1}{(2T_x)^2}\mathrm{Var}[Z_T(x + T_x, y) - Z_T(x - T_x, y)] = \frac{1}{2T_x^2}\{E[Z_T^2] - E[Z_T(x + T_x, y)Z_T(x - T_x, y)]\}$$

Given the following identities:

$$(10) \qquad \sigma_{Z_T}^2 = E[Z_T^2] - E^2[Z_T]$$

$$\sigma^2_{Z_T}\rho_{Z_T}(2T) = \mathrm{E}[Z_T(x+T,y)Z_T(x-T,y)] - \mathrm{E}^2[Z_T] \tag{11}$$

eq. (9) can be simplified to be

$$\sigma^2_{S_{Tx}} = \frac{\sigma^2_{Z_T}}{2T_x^2}[1-\rho_{Z_T}(2T_x)] \simeq \frac{\sigma^2_{Z_T}}{2T_x^2}[1-\rho_Z(2T_x)] \tag{12}$$

where σ_{Z_T} represents the standard deviation of the observed elevation data (i.e., at the DEM scale), $\mathrm{E}[Z_T]$ represents the expected value of Z_T, and $\rho_{Z_T}(2T)$ represents the Gaussian two-dimensional correlation function between the DEM local averages. A similar set of equations exists for the variance of S_{T_y}, simply by substituting the subscript x with y.

In detail, $\rho_{Z_T}(2T_x)$ is the average of the correlation coefficient between every pair of actual elevation points contained within two DEM cells separated by central distance $2T_x$ (or $2T_y$ in the y direction). This correlation was approximated in eq. (12) by assuming that $\rho_{Z_T}(2T_x) \simeq \rho_Z(2T_x)$, where ρ_Z is the correlation coefficient between elevation points. In other words, the correlation between local averages is approximated by the correlation between their centers, leading to the right side of eq. (12). This is a reasonable approximation if the actual correlation function does not vary too rapidly around $2T$, which is generally the case if the correlation length is larger than the DEM cell size.

This research adopts a Gaussian correlation structure, rather than the perhaps more common Markovian correlation structure, because the resulting random field is mean square differentiable, meaning that its derivates (i.e., slopes) have finite variance. Mean square differentiability simplifies the model mathematically by ensuring that the slope variance remains finite as the averaging dimension decreases to zero, which is also physically more realistic.

If $Z(x, y)$ has a Gaussian correlation structure, its correlation function, $\rho_Z(\tau_x, \tau_y)$, is as follows (see, e.g., Fenton and Griffiths 2008):

$$\begin{aligned}\rho_Z(\tau_x,\tau_y) &= \exp\left\{-\pi\left[\left(\frac{\tau_x}{\theta_{Z_x}}\right)^2+\left(\frac{\tau_y}{\theta_{Z_y}}\right)^2\right]\right\} \\ &= \exp\left[-\pi\left(\frac{\tau_x}{\theta_{Z_x}}\right)^2\right]\exp\left[-\pi\left(\frac{\tau_y}{\theta_{Z_y}}\right)^2\right]\end{aligned} \tag{13}$$

where τ_x and τ_y are the directional separation distances between two points in the domain, and θ_{Z_x} and θ_{Z_y} are the directional correlation lengths. The correlation length is used to describe the degree of linear dependence between elevations. For example, consider any two elevation points separated by distance τ; as the points are shifted around, if the elevation of one doubles, and the elevation of the other tends to do so as well, then points separated by distance τ are strongly positively correlated. This typically occurs when τ is small (i.e., the points are close together). The correlation length may be roughly viewed as the separation distance beyond which the two points will be largely uncorrelated. Thus, the smaller the correlation length, the more erratic the elevation profile, as seen in a mountainous region (because of more independence between elevations).

The correlation function given by eq. (13) is separable, and if $\theta_{Z_x} = \theta_{Z_y} = \theta_Z$, then the correlation function is also isotropic. Assuming isotropy holds, the correlation function simplifies as follows:

$$\rho_Z(\tau_x,\tau_y) = \exp\left[-\frac{\pi}{\theta_Z^2}(\tau_x^2+\tau_y^2)\right] \tag{14}$$

Letting $\tau = \sqrt{\tau_x^2+\tau_y^2}$ be the absolute distance between any two points, the correlation function can be written as

$$\rho_Z(\tau) = \exp\left[-\pi\left(\frac{\tau}{\theta_Z}\right)^2\right] \tag{15}$$

which allows eq. (12) to be expressed as

$$\sigma^2_{S_T} \simeq \frac{\sigma^2_{Z_T}}{2T^2}\left\{1-\exp\left[-\pi\left(\frac{2T}{\theta_Z}\right)^2\right]\right\} \tag{16}$$

where T is either T_x or T_y and where θ_Z is the correlation length between elevation points, Z. The approximation in eq. (16) is because the correlation between local averages is approximated by correlation between local average centers, as discussed earlier. The two remaining unknowns in eq. (16), the correlation length, θ_Z, and the standard deviation of the locally averaged elevation data (e.g., at the DEM or critical scales), σ_{Z_T}, can be determined using local averaging theory along with data from two DEMs (each covering the same region).

According to local averaging theory (Vanmarcke 1984), a relationship exists between the standard deviation of the perceived (locally averaged) elevation data, σ_{Z_T}, and the standard deviation of the true elevation data, σ_Z,

$$\sigma^2_{Z_T} = \sigma_Z^2\gamma_Z(T_x,T_y) \tag{17}$$

where $\gamma_Z(T_x, T_y)$ is a variance reduction function describing the amount that the variance is reduced when the elevation is averaged over the cell domain, $T_x \times T_y$. The value of $\gamma_Z(T_x, T_y)$ decreases from one to zero as $T_x \times T_y$ increases.

If $Z(x, y)$ has a Gaussian correlation structure, as assumed, the Gaussian variance function, $\gamma_Z(T_x, T_y)$, can be expressed as follows (Fenton and Griffiths 2008):

$$\begin{aligned}\gamma_Z(T_x,T_y) &= \frac{\theta^2_{Z_x}}{\pi T_x^2}\left[\frac{\pi T_x}{\theta_{Z_x}}\mathrm{erf}\left(\frac{\sqrt{\pi}T_x}{\theta_{Z_x}}\right)+\exp\left(\frac{-\pi T_x^2}{\theta^2_{Z_x}}\right)-1\right] \\ &\times \frac{\theta^2_{Z_y}}{\pi T_y^2}\left[\frac{\pi T_y}{\theta_{Z_y}}\mathrm{erf}\left(\frac{\sqrt{\pi}T_y}{\theta_{Z_y}}\right)+\exp\left(\frac{-\pi T_y^2}{\theta^2_{Z_y}}\right)-1\right] = \gamma_Z(T_x)\gamma_Z(T_y)\end{aligned} \tag{18}$$

Because the correlation function is separable and assumed isotropic, the variance reduction function is also separable and isotropic, and can be simplified to

$$\gamma_Z(T,T) = \gamma_Z^2(T) \tag{19}$$

if $T_x = T_y = T$. The approximation $T = \sqrt{T_xT_y}$ gives fairly good variance reduction function results, in the event that $T_x \neq T_y$, if the correlation structure is approximately isotropic and if T_x and T_y do not differ excessively (e.g., by more than about a factor of two). In this case,

$$\gamma_Z(T) = \frac{\theta_Z^2}{\pi T^2}\left[\frac{\pi T}{\theta_Z}\mathrm{erf}\left(\frac{\sqrt{\pi}T}{\theta_Z}\right)+\exp\left(\frac{-\pi T^2}{\theta_Z^2}\right)-1\right] \tag{20}$$

Now let T_1 represent the cell dimension of one of the DEMs, and T_2 the cell dimension of the other. If the cells are not square, the approximation $T_1 = \sqrt{T_xT_y}$ can be used, as discussed earlier, and similarly for T_2. Each cell experiences some degree of local aver-

aging, the extent of which is dependent upon the cell dimension T_i, $i = 1, 2$, and the standard deviation of the cell elevation emerges from eqs. (17), (19), and (20), as follows:

$$(21a) \qquad \sigma_{Z_{T_1}} = \sigma_Z \gamma_Z(T_1)$$

$$(21b) \qquad \sigma_{Z_{T_2}} = \sigma_Z \gamma_Z(T_2)$$

The values of $\sigma_{Z_{T_1}}$ and $\sigma_{Z_{T_2}}$ can be determined through a statistical analysis of each of the DEM datasets and then the point scale standard deviation, σ_Z, can be eliminated by taking the ratio of eqs. [21*a*] and [21*b*]. The resulting ratio can be used to solve iteratively for the point scale correlation length, θ_Z, by finding θ_Z, which satisfies the following equation:

$$(22) \qquad \frac{\sigma_{Z_{T_1}}}{\sigma_{Z_{T_2}}} = \frac{\gamma_Z(T_1)}{\gamma_Z(T_2)} = \frac{\theta_Z^2}{\pi T_1^2}\left[\frac{\pi T_1}{\theta_Z}\mathrm{erf}\left(\frac{\sqrt{\pi}T_1}{\theta_Z}\right) + \exp\left(\frac{-\pi T_1^2}{\theta_Z^2}\right) - 1\right] \times \left\{\frac{\theta_Z^2}{\pi T_2^2}\left[\frac{\pi T_2}{\theta_Z}\mathrm{erf}\left(\frac{\sqrt{\pi}T_2}{\theta_Z}\right) + \exp\left(\frac{-\pi T_2^2}{\theta_Z^2}\right) - 1\right]\right\}^{-1}$$

By substituting the resulting value of θ_Z back into eq. (20), separately for each DEM (i.e., for T_1 and T_2), the values of $\gamma_Z(T_1)$ and $\gamma_Z(T_2)$ can be determined. Then the following equation (which is simply a rearrangement of eq. (17)) can be used to calculate the point scale standard deviation of the elevation data, σ_Z,

$$(23) \qquad \sigma_Z = \frac{\sigma_{Z_T}}{\gamma_Z(T)}$$

using the values of σ_{Z_T} and $\gamma_Z(T)$ at either DEM resolution (or using an average of the two).

As previously discussed, the critical scale refers to the minimum cell size at which a single slope failure is considered hazardous. There is little value in considering cell sizes below the critical scale because slope failures at those scales are not deemed to be hazardous. The critical scale then is the scale that this study will concentrate on as the most conservative indicator of regional landslide hazard. As a result, eqs. (16) and (21) can be used to solve for the standard deviation of the slope angles at the critical scale, that is,

$$(24) \qquad \sigma_{S_{T_{crit}}} \simeq \frac{\sigma_Z \gamma_Z(T_{crit})}{T_{crit}\sqrt{2}}\sqrt{1 - \exp\left[-\pi\left(\frac{2T_{crit}}{\theta_Z}\right)^2\right]}$$

where T_{crit} is selected based upon expert judgement and may vary from region to region. Returning to eq. (8), the distribution of maximum slope angles can now be evaluated using the value of $\sigma_{S_{T_{crit}}}$, as estimated in eq. (24).

Conditional probability of slope failure

To assess the conditional probability of slope failure, given the slope angle, the spatial variability of the ground strength in a slope must be considered. One way of doing this is to model the ground as a spatially varying random field and then use a finite element analysis to determine whether realizations of the slope fail or not. The resulting random finite element method developed by Fenton and Griffiths (2008) uses the site-specific soil properties (friction angle, dilation angle, cohesion, unit weight, elastic modulus, and Poisson's ratio) and slope geometry to estimate the probability of failure of a slope having a given slope angle. This conditional probability of failure (for given slope angle) can be estimated using the 2D stochastic slope stability analysis program, Rslope2d, developed by Griffiths and Fenton (2000, 2004). Rslope2d generates a random field of soil properties, assigns property values to each element, applies gravity loading, and monitors the stress at all Gauss points. If there is excess stress at any point, the program attempts to redistribute it to nearby points to satisfy the maximum allowable stress limitations, as specified by a Mohr–Coulomb failure criterion. If, after a maximum number of iterations, Rslope2d is not able to successfully redistribute the stress, the slope is considered to have failed (Griffiths et al. 2009). This overall approach is referred to as the random finite element method (RFEM) because it combines elastoplastic finite element analysis with a random field generator, simulated via the local average subdivision method (Fenton and Vanmarcke 1990). By varying the slope angle in Rslope2d, it is possible to observe the relationship between the slope angle and the probability of slope failure. Thus, the results of Rslope2d, when executed for various slope angles, can be used to derive a relationship predicting the probability of slope failure for any of the possible slope angles, s_i (where s_i is interpreted here as being at the midpoint of its range).

The ground strength parameters used in the RFEM model should be those that represent the minimum strength (because of rainfall and (or) seismic events, for example) over the target lifetime of the risk assessment. These parameters will likely vary throughout the region under analysis. Therefore, a range of soil conditions should be considered spatially and the weakest values expected to occur over time should be assumed at each spatial point. For example, if a region were composed primarily of two types of soil, Rslope2d would be implemented in two sets of probabilistic analyses, one for each soil type over all possible slope angles. The final conditional failure probability of a randomly selected slope in the region would be a weighted average of these two probability distributions, the weights being the relative proportions of the two soil types in the region. In detail, for a region composed of n_s different soil types, the final slope failure probability would be given by the total probability theorem as

$$(25) \qquad P[F_1|S_{T_m} = s_i] = \sum_{k=1}^{n_s} p_k r_{ki}$$

where F_1 is the event that a single randomly selected slope fails, p_k is the proportion of the region having the kth soil type, and r_{ki} is the failure probability of the kth soil type at the slope angle s_i, as estimated by Rslope2d. Thus, the probability given by eq. (25) is the conditional probability that a randomly selected slope having slope angle s_i fails.

Regional landslide hazard assessment

Because a region is generally composed of many individual slopes, the *regional* landslide hazard level here refers to the probability of one or more slopes failing in the region. Therefore, attention should now be turned to calculating the probability of *at least* one slope failure throughout an entire region of some areal extent, A_t. If the area is large, then it will consist of possibly very many separate slopes. For simplicity, assume that a typical slope in the region has areal dimensions $T \times T$. If this is so, then the number of slopes having maximum slope angle, s_i, in the region will be approximately

$$(26) \qquad n_i \simeq n_t P[S_{T_m} = s_i] = \left(\frac{A_t}{T^2}\right)P[S_{T_m} = s_i]$$

where $n_t = A_t/T^2$ is the total number of slopes in the region A_t. Note that n_i is actually random (having a binomial distribution), but is taken to be equal to its mean in eq. (26) — hence the approxima-

tion in eq. (26). This is a reasonable approximation because n_i is usually large and because $P[S_{T_m} = s_i]$ is generally estimated directly from the region being studied.

Letting N_{n_i} be the random number of slopes that fail out the n_i slopes having slope angle s_i, then the probability that one or more of these slopes fail is $P[N_{n_i} \geq 1]$. As this probability increases, the general landslide hazard level of the region will clearly also increase. Assuming independence between the n_i slopes, each having slope angle s_i, and that the probability of slope failure is $P[F_1|S_{T_m} = s_i]$ (see eq. (25)), then the probability of at least one slope failure from these slopes is given by

$$P[N_{n_i} \geq 1] = 1 - P[N_{n_i} = 0] = 1 - q_i^{n_i} \tag{27}$$

where q_i is the probability of nonfailure of a slope having slope angle s_i,

$$q_i = 1 - P[F_1|S_{T_m} = s_i] = 1 - \sum_{k=1}^{n_s} p_k r_{ki} \tag{28}$$

The assumption that slopes fail independently with constant failure probability $P[F_1|S_{T_m} = s_i]$ means that N_{n_i} follows a binomial distribution. Admittedly, the assumption of independence is not particularly reasonable. For example, if an earthquake strikes the region, it is more likely that several slopes will fail simultaneously — the common cause being the earthquake. However, the assumption of independence is *conservative*, in the sense that it leads to a higher probability of regional failure than if the slope failures are positively correlated (i.e., if one fails, others are more likely to fail). Thus, eq. (27) provides a conservative measure of the landslide susceptibility over a region. It should also be noted that this measure depends on the size of the region, A_t. As A_t goes to infinity, the number of slopes involved also goes to infinity, and the regional probability of slope failure goes to one (i.e., $P[N_{n_i} \geq 1] \rightarrow 1$). This makes sense in that it is to be expected that at least one slope failure will occur in very large areas.

In summary, the regional landslide hazard level, p_f, defined as the probability of failure of at least one slope throughout the region, A_t, can be computed using the total probability theorem over the range of possible slope angles as

$$p_f = \sum_{s_i = s_{min}}^{s_{max}} (1 - q_i^{n_i}) P[S_{T_m} = s_i] \tag{29}$$

where n_i is given by eq. (26), q_i is given by eq. (28), and $P[S_{T_m} = s_i]$ is given by eq. (8).

Landslide magnitude

By comparing the regional landslide hazard levels at various resolutions, it is also possible to break the regional failure probability down by landslide magnitude. For example, eq. (29) may predict a 50% regional failure probability of slopes of size $T = 10$ m. As the averaging dimension increases, small slopes are filtered out in favour of larger slopes. In essence, an averaging domain of size $T = 100$ m is effectively concentrating on slopes of dimension 100 m, the smaller slopes being averaged out.

As will be shown in the next section, the regional failure probability decreases as the averaging dimension, T, increases. For example, eq. (29) may predict a regional failure probability of 30% for slopes of size $T = 100$ m while only 2% for slopes of size $T = 1000$ m. In other words, the theory given earlier can be used to estimate the relative likelihood of different sizes of landslides (e.g., 10 m slides versus 1000 m slides). Although not pursued in this paper, the presented relationship between landslide size and its probability of occurrence allows for a more complete regional risk assessment integrating failure probabilities with failure consequences.

Table 1. Digital elevation model measurement parameters.

	GTOPO (T_1)	SRTM (T_2)
Number of cells in x direction	48	470
Number of cells in y direction	52	514
Latitude of region's lower left corner (°)	45.683 33	45.683 33
Longitude of region's lower left corner (°)	6.675 00	6.681 67
Cell size = $\Delta_{lat} = \Delta_{long}$ (°)	0.008 33	0.000 83

Case study

A 31 km × 48 km region in the Alps, near Chamonix, France, has been selected to illustrate the regional landslide hazard assessment methodology presented in this paper. The test site is composed of mountainous terrain ranging from 459 to 4784 m in elevation which has been previously mapped by two different DEMs: (*i*) the global 30 arc-second elevation (GTOPO) model; and (*ii*) the shuttle radar topography mission (SRTM) model with 3 arc-second resolution (see Table 1). There is a significant difference in level of detail perceived by these two models (see Figs. 1 and 2). Note that the results of this paper do not depend on the types of DEMs employed, as long as they have different resolutions, because all DEMs involve some degree of local averaging.

The GTOPO30 documentation (Gesch and Greenlee 1997) suggests that the 90% confidence interval on absolute elevations derived from the GTOPO model is ±30 m, but they go on to say that the "relative accuracy is probably better than estimated absolute accuracy" and it is the relative accuracy that is important for slope computations. Similarly, the SRTM homepage (JPL 2009) suggests that the 90% confidence interval on absolute elevations derived from the SRTM model is ±5 m, again with better relative accuracy. For both models, it will be assumed here that the relative elevation errors are mean zero and not large enough to result in a significant change to the slope angle *distributions* estimated from the DEMs in this case study. It is believed that this is a reasonable assumption.

Because of the spherical nature of the Earth, the size of a standard DEM cell is dependent upon its geographic coordinates (Zhang et al. 1999). The dimensions can be computed using the Haversine formula (Smith et al. 2007):

$$T = 2r_E \arcsin\sqrt{\sin^2\left(\frac{\Delta_{lat}}{2}\right) + \cos(L_1)\cos(L_2)\sin^2\left(\frac{\Delta_{long}}{2}\right)} \tag{30}$$

where r_E is the radius of the Earth, which is approximately 6371 km (NIMA 2000), L_1 and L_2 are the latitudinal coordinates on the Earth's surface of the cell edges, Δ_{lat} is the difference between the two latitudinal coordinates of the cell edges, and Δ_{long} is the difference between the two cell edge longitudinal coordinates.

Because the test region is small in comparison to the Earth, each cell is assumed to be the same size, relative to the central cell. According to eq. (30), the GTOPO central cell dimensions are $T_x = 644.97$ and $T_y = 926.59$, with an equivalent "square cell" dimension of $T_1 = 773.06$ m. The SRTM cell dimensions are $T_x = 64.50$ and $T_y = 92.66$ with an equivalent "square cell" dimension of $T_2 = 77.31$ m. Very similar dimensions are found for any cell in the region, differing by no more than 0.1% from the central cell.

Fig. 1. GTOPO coverage of test region (image courtesy of the Norwegian Geotechnical Institute) (644.97 m × 926.59 m cells).

Fig. 2. SRTM coverage of test region (image courtesy of the Norwegian Geotechnical Institute) (64.50 m × 92.66 m cells).

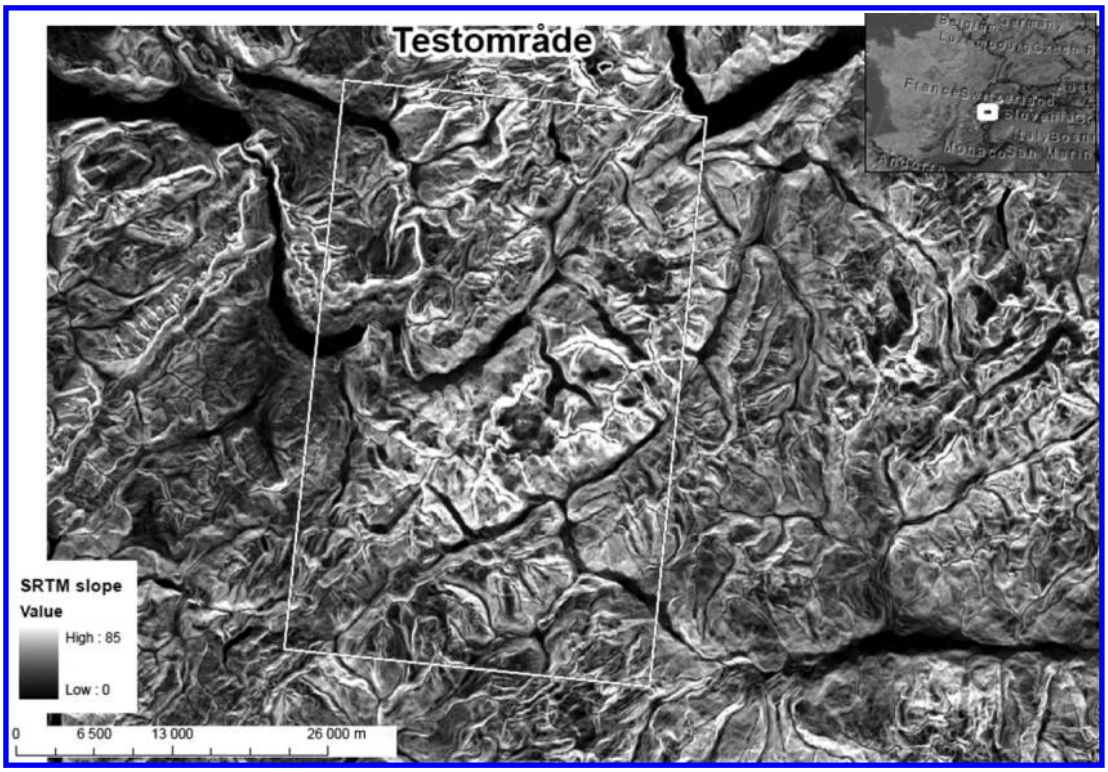

Distribution of maximum slope angle

Based on a statistical analysis of the DEM elevation data provided for this case study, the following perceived standard deviations are estimated: $\sigma_{Z_{T_1}} = 678.08$ m and $\sigma_{Z_{T_2}} = 702.57$ m (see Fig. 3). As expected, the variance of the higher resolution model is larger than the variance of the lower resolution model because its smaller cells are less obscured by the effects of local averaging.

Equation (22), which employs local averaging theory, can now be used with the values of $\sigma_{Z_{T_1}}$ and $\sigma_{Z_{T_2}}$ to solve for the point scale correlation length of the elevation data,

Fig. 3. Histograms of elevation data collected by the GTOPO and SRTM DEMs.

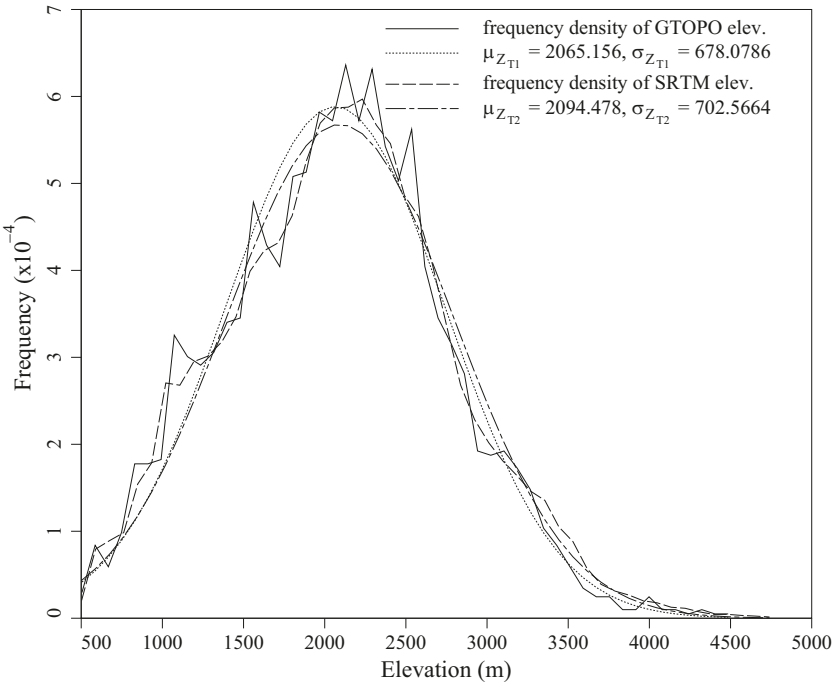

$$(31)\qquad \frac{678.08}{702.57} = \frac{\gamma_Z(T_1)}{\gamma_Z(T_2)} = \left(\frac{\theta_Z^2}{773.06\pi}\right)\left(\frac{773.06\pi}{\theta_Z}\operatorname{erf}\left\{\frac{773.06\sqrt{\pi}}{\theta_Z}\right\} + \exp\left\{\frac{-773.06^2\pi}{\theta_Z^2}\right\} - 1\right) \times \left\{\left(\frac{\theta_Z^2}{77.31\pi}\right)\left[\frac{77.31\pi}{\theta_Z}\operatorname{erf}\left(\frac{77.31\sqrt{\pi}}{\theta_Z}\right) + \exp\left(\frac{-77.31^2\pi}{\theta_Z^2}\right) - 1\right]\right\}^{-1}$$

which gives θ_z = 2917 m. This value of θ_Z implies that, throughout the region, elevation points separated by more than 2917 m in the plane are negligibly correlated with one another.

The point scale standard deviation of the elevation data, σ_Z, can be evaluated by substituting the variance functions for each of the DEMs (calculated with eq. (20)) into eq. (23) as follows:

$$(32a)\qquad \gamma_Z(T_1) = \frac{2917^2}{773.06^2\pi}\left[\frac{773.06\pi}{2917}\operatorname{erf}\left(\frac{773.06\sqrt{\pi}}{2917}\right) + \exp\left(\frac{-773.06^2\pi}{2917^2}\right) - 1\right] = 0.9648$$

$$(32b)\qquad \gamma_Z(T_2) = \frac{2917^2}{77.31^2\pi}\left[\frac{77.31\pi}{2917}\operatorname{erf}\left(\frac{77.31\sqrt{\pi}}{2917}\right) + \exp\left(\frac{-77.31^2\pi}{2917^2}\right) - 1\right] = 0.9996$$

$$(33)\qquad \sigma_Z = \sigma_{Z_1} = \sigma_{Z_2} = \frac{678.08}{0.9648} = \frac{702.57}{0.9996} = 702.83 \text{ m}$$

The standard deviation of the elevation data at the point scale is higher than for each of the DEMs as it is unaffected by local averaging.

Now that both the correlation length and standard deviation of the elevation data have been estimated at the point scale, the distribution of slope angles perceived at the critical scale can be estimated. For this case study, a critical scale of 10 m has been chosen arbitrarily, as discussed in the Introduction. Furthermore, because the point scale correlation length (2917 m) is very much larger than the scale under consideration (10 m), $\gamma(T_{crit})$ will be very close to 1.0 so that it can be ignored in eq. (24). This gives,

$$(34)\qquad \sigma_{S_{T_{crit}}} = \frac{702.83}{10\sqrt{2}}\sqrt{1 - \exp\left\{-\pi\left[\frac{2(10)}{2917}\right]^2\right\}} = 0.603\,932 \simeq 0.604$$

Although the averaging dimension of the critical scale was chosen arbitrarily, the dimension does not affect the resulting value of $\sigma_{S_{T_{crit}}}$ very much. For example, if T_{crit} were chosen to be a smaller value (e.g., 1 m), then $\sigma_{S_{T_{crit}}}$ = 0.603 953, or a larger value (e.g., 20 m), then $\sigma_{S_{T_{crit}}}$ = 0.603 865.

Equation (8) can now be used to determine the distribution of perceived maximum slope angles at the critical scale,

$$(35)\qquad P\left[S_{T_{m_{crit}}} = s_i\right] = \exp\left[-\frac{s_{i-}^2}{2(0.604)^2}\right] - \exp\left[-\frac{s_{i+}^2}{2(0.604)^2}\right]$$

where s_{i-} and s_{i+} are defined by eq. (6).

Conditional probability of slope failure

To illustrate how to apply the proposed regional landslide hazard assessment methodology, a relatively simple problem is considered where the soil types present in the test region have been chosen arbitrarily as p_1 = 20% fine-grained soils (soil type 1) and p_2 = 80% gravely sands (soil type 2). The values of the individual ground strength parameters assumed are shown in Tables 2 and 3.

Table 2. Assumed ground strength parameters of fine-grained soils (soil type 1).

	Assumed values		
Ground strength parameters	Mean	Standard deviation	Distribution type
Friction angle (°)	26	5	Bounded
Dilation angle (°)	0	0	Deterministic
Cohesion (kN)	0	0	Deterministic
Unit weight (kN/m³)	13	1.5	Lognormal
Elastic modulus (kPa)	20 000	15 000	Lognormal
Poisson's ratio	0.3	0	Deterministic

Table 3. Assumed ground strength parameters of gravely sands (soil type 2).

	Assumed values		
Ground strength parameters	Mean	Standard deviation	Distribution type
Friction angle (°)	40	5	Bounded
Dilation angle (°)	0	0	Deterministic
Cohesion (kN)	0	0	Deterministic
Unit weight (kN/m³)	18	1	Lognormal
Elastic modulus (kPa)	125 000	75 000	Lognormal
Poisson's ratio	0.3	0	Deterministic

The fact that only frictional soil types were considered was an arbitrary decision, made purely to illustrate the theoretical model, and so the results of this case study should not be considered to reflect the actual landslide hazard level of the region. The methodology would apply for any ground types and any parameter choices made in Tables 2 and 3, but will give different results as these parameters are changed.

Assuming that the ground strength parameters identified in Tables 2 and 3 are representative of the ground over the region being considered (at their resident proportions) the conditional failure distribution, $P[F_1|S_{T_m} = s_i]$, can be estimated by running Rslope2d over a range of possible slope angles. The actual slope geometries used in the Rslope2d model varied with the slope angle. When the slope angle was $s = 1.0$ (45°), the slope height used was 30 m (reducing for shallower slopes). The overall model length in the horizontal direction when $s = 1.0$ was 130 m (including head and toe regions). Because the estimated (and worst case) correlation length between soil properties is generally some fraction of the soil model dimension, the soil correlation length assumed here was 10% of the overall soil model length. Thus, the soil correlation length in this case study was assumed to be 13 m and isotropic. This is believed to be reasonably conservative. The choice of a 30 m slope height, in the case where $s = 1.0$, was rather arbitrary. However, because most slope angles perceived by the higher resolution DEM (SRTM) are less than $s = 0.5$ m/m (as seen later), a characteristic slope height for the SRTM should be less than $0.5 \times T_2 = 0.5(77.3) = 38.7$ m, if the assumption made earlier that each slope has plan dimension T_2 is deemed reasonable. Thus, a 30 m slope height was assumed to be reasonable for the determination of individual slope failure probabilities.

For each set of parameters of the two ground types considered here, Rslope2d was run over a range of slope angles, $s_i = \tan(d_i)$, for $i = 0, 1, \ldots, 89$, to yield estimates of $P[F_1|S = s_i]$ and these probabilities are plotted in Fig. 4. Not surprisingly, the slope failure probability increases from 0 to 1 as the slope angle increases. Somewhat more surprising is the fact that the increase almost exactly follows a suitably selected standard normal cumulative distribution function, Φ. For cohesionless soils (as assumed here), the probability of slope failure is equal to the probability that the slope gradient exceeds the friction angle, so if the friction angle distribution resembles a normal distribution, the failure probability will be closely normal. For the relatively small standard deviations of the friction angle (relative to the means) assumed in Tables 2 and 3, the friction angle distribution resembles a normal distribution (although it is actually bounded). The fitted cumulative normal distribution functions are also shown in Fig. 4. The fit was made by trial and error for both the fine-grained (type 1) and gravely soils (type 2) and are as follows:

$$r_{1i} \simeq \Phi\left(\frac{s_i - 0.505}{0.025}\right) \tag{36a}$$

$$r_{2i} \simeq \Phi\left(\frac{s_i - 0.874}{0.035}\right) \tag{36b}$$

where subscripts 1 and 2 refer to fine-grained soils and gravely sands, respectively (see eq. (25)).

Regional landslide hazard assessment at critical scale

Using eqs. (28) and (29), the overall regional probability of slope failure (i.e., regional landslide hazard level) at the critical scale can be expressed as

$$p_f = \sum_{s_i = s_{min}}^{s_{max}} \left[1 - \left(1 - \sum_{k=1}^{n_s} p_k r_{ki}\right)^{n_i}\right] P[S_{T_m} = s_i] \tag{37}$$

where the values of r_{ki} are given by eq. (36), $P[S_{T_m} = s_i]$ is given by eq. (35) (with $T_m = T_{m_{crit}}$), and n_i is given by eq. (26).

It is assumed that $n_s = 2$, $p_1 = 0.2$, $p_2 = 0.8$ (see Tables 2 and 3), and $n_i = n_t P[S_{T_m} = s_i]$, where $n_t = A_t/T^2$ and $A_t = (64.50 \times 470) \times (92.66 \times 514) = 1.444 \times 10^9$ m² (based on the SRTM DEM). This means that at the critical scale where $T = T_{crit} = 10$ m, the number of slopes at each possible slope angle is $n_i = 1.444 \times 10^7\ P[S_{T_m} = s_i]$ and so the regional slope failure probability can be estimated at the critical scale to be,

$$p_f = \sum_{s_i = s_{min}}^{s_{max}} \left\{1 - \left[1 - 0.2\Phi\left(\frac{s_i - 0.505}{0.025}\right) - 0.8\Phi\left(\frac{s_i - 0.874}{0.035}\right)\right]^{n_i}\right\} P[S_{T_m} = s_i] = 0.805 \tag{38}$$

This value of p_f implies that there is a 80.5% probability of at least one slope of size $T_{crit} = 10$ m (or greater) failing in the region. Note the lack of time dependence in this estimate. The time dependence is implicitly included in the ground strength parameters listed in Tables 2 and 3, which are to be interpreted as being the lowest strength values that will occur over the time duration of interest (e.g., the next 100 years).

Regional landslide hazard assessment at DEM resolutions

The slope angle distributions derived from the two DEM datasets (using eqs. [2a] and [2b]) are plotted in Figs. 5 and 6. The standard deviations of the slope angles are assumed to be equal in each of the x and y directions (see the "Distribution of maximum slope angle" section for details), so that $\sigma_{S_{T_1}}$ is taken as the average of $\sigma_{S_{T_{1x}}}$ and $\sigma_{S_{T_{1y}}}$ (and similarly for $\sigma_{S_{T_2}}$),

$$\sigma_{S_{T_1}} \simeq \frac{\sigma_{S_{T_{1x}}} + \sigma_{S_{T_{1y}}}}{2} = \frac{0.279\,230 + 0.238\,303}{2} \simeq 0.259 \tag{39a}$$

$$\sigma_{S_{T_2}} \simeq \frac{\sigma_{S_{T_{2x}}} + \sigma_{S_{T_{2y}}}}{2} = \frac{0.463\,691 + 0.436\,291}{2} \simeq 0.450 \tag{39b}$$

Fig. 4. Conditional probability of failure plots for fine-grained soils and gravely sands.

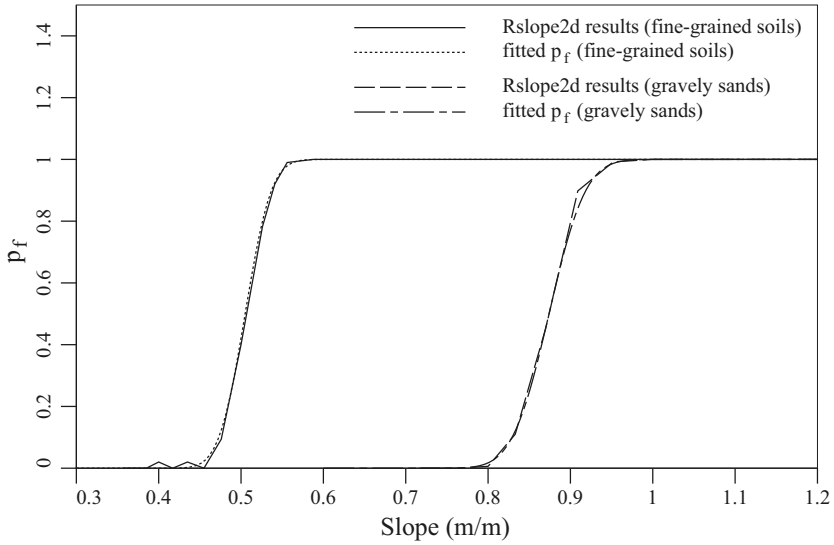

Fig. 5. Histogram of slope angles as perceived by the GTOPO DEM.

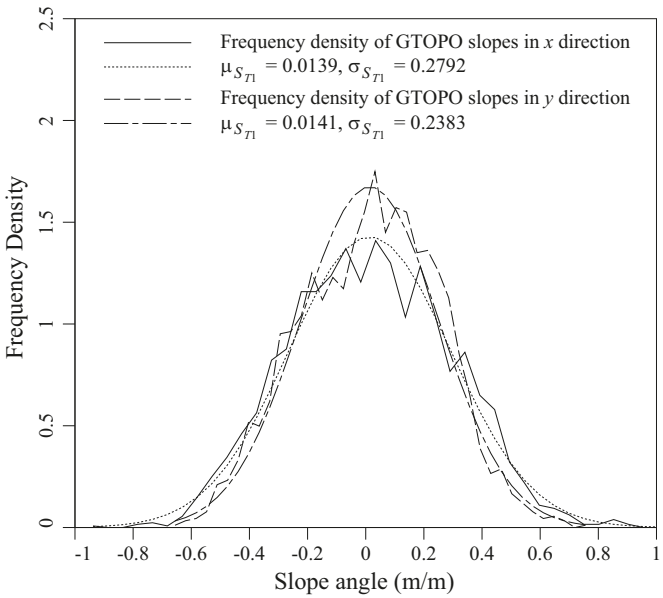

Fig. 6. Histogram of slope angles as perceived by the SRTM DEM.

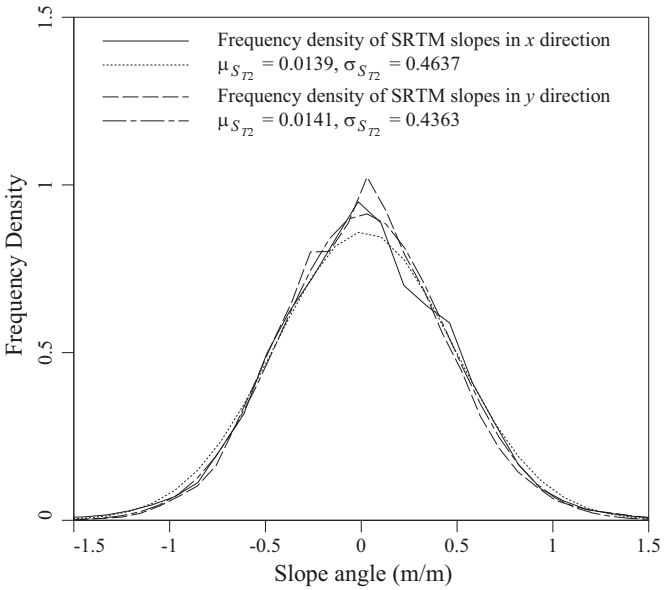

Given the values of $\sigma_{S_{T_1}}$ and $\sigma_{S_{T_2}}$, the distributions of maximum slope angles, as perceived by each of the DEMs, can be determined using eq. (8).

$$(40a)\qquad P[S_{T_{m1}} = s_i] = \exp\left[-\frac{s_{i-}^2}{2(0.259)^2}\right] - \exp\left[-\frac{s_{i+}^2}{2(0.259)^2}\right]$$

$$(40b)\qquad P[S_{T_{m2}} = s_i] = \exp\left[-\frac{s_{i-}^2}{2(0.450)^2}\right] - \exp\left[-\frac{s_{i-}^2}{2(0.450)^2}\right]$$

The slope failure probabilities r_{ki} (see eq. (36)) used for the critical scale analysis also apply to the DEM scale analyses. Therefore, the regional landslide failure probabilities, as perceived at each of the DEM resolutions, can be evaluated with eq. (37) by using the appropriate distribution $P[S_{T_m} = s_i]$ and by modifying $n_t = (A_t/T^2)$ using $T = T_1 = 773.06$ for the GTOPO scale or $T = T_2 = 77.31$ for the SRTM scale. This gives $n_t = 2416$ for the GTOPO scale and 241 599 for the SRTM scale.

The final regional probabilities of slope failure, p_{f_1} for the GTOPO scale and p_{f_2} for the SRTM scale, are found via eq. (37) to be

$$(41)\qquad p_{f_1} = 0.201 \quad \text{and} \quad p_{f_2} = 0.644$$

The slope angle probability distributions (see eqs. (8), (35), and (40)) perceived at each of the three scales are shown in Fig. 7. The figure clearly shows how both the mean and variance increase as the resolution increases (i.e., as the averaging scale decreases).

The GTOPO DEM, which has the lowest resolution, estimates the lowest regional probability of slope failure at about 20%. The SRTM DEM, which is significantly more precise than the GTOPO DEM, estimates a much higher 64% regional probability of slope failure. In comparison, the critical scale model estimates the highest failure probability at 81%. Two conclusions can be drawn from these results.

First of all, these results suggest that it is moderately unlikely that a slope greater than $T_1 = 773$ m will fail (about 20%), but moderately likely that a slope greater than $T_2 = 77.3$ m will fail (64%) and highly likely that a slope greater than 10 m will fail (81%).

Fig. 7. GTOPO, SRTM, and critical scale slope angle distributions (eq. (8)).

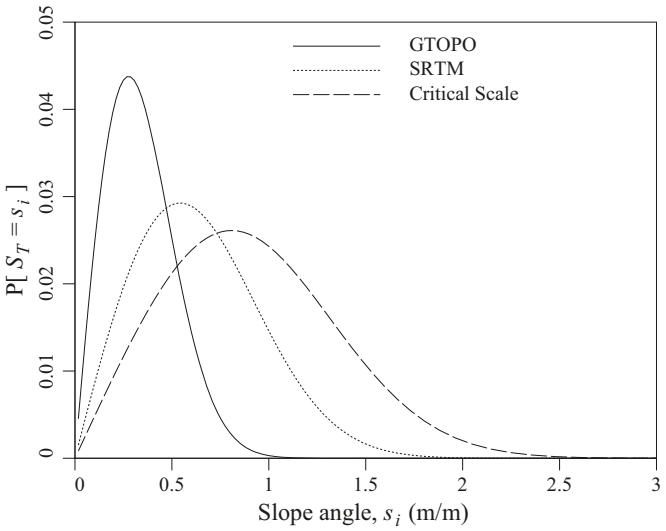

This information can be used for detailed risk assessments that consider the frequency versus consequences (how much damage is expected to occur) for landslides of different sizes. For instance, it might be pragmatic to invest in contingency plans for landslides up to (or even slightly larger than) roughly 500 m in scope. However, if resources are limited, it may not be practical to prepare for landslides larger than about 1000 m because they appear to be unlikely to occur.

Secondly, low resolution DEMs generally underestimate landslide hazard levels as a result of local averaging. If more accurate predictions of regional slope failure are not available (e.g., at the critical scale), the unrealistically low landslide hazard levels estimated by low resolution DEMs could result in inadequate levels of landslide planning and preparation. The lowest resolution DEM (GTOPO) used in this case study has very large cells and the perceived slope angles, S_{T_1}, are significantly underestimated. The slope angles, S_{T_2}, perceived by the SRTM DEM, and $S_{T_{crit}}$, estimated at the critical scale, are also underestimated, but to lesser and lesser degrees.

Concluding remarks

The landslide hazard model developed in this paper estimates the probability, p_f, of at least one slope failing in a region. The regional slope failure probability estimate takes into account the distribution of maximum slope angles and the conditional probabilities of slope failures as a function of ground conditions. The probability, p_f, is used as a measure of the regional landslide hazard level.

Because there is only one elevation recorded for each DEM cell, the ability of the recording to accurately reflect the nature of the terrain is directly related to the cell size. The larger the cell, the more local averaging takes place within the cell and the less accurate the representation of the terrain's true roughness. Typically, steep slopes that are small in spatial extent are overlooked by low resolution DEMs as a result of local averaging. Unfortunately, many of these small steep slopes often present high probabilities of slope failure, and if they are not considered by a DEM, the regional landslide hazard level will be underestimated. This can create serious issues for landslide preparedness planning. In other words, important precautions, such as emergency response procedures and construction regulations, may be neglected if the landslide hazard level is underestimated.

To reduce the inaccuracies resulting from the effects of local averaging on a DEM, the landslide hazard level should be estimated over a variety of scales, starting with the most conservative at the critical scale. The critical scale refers to the minimum scale at which a landslide would be deemed hazardous. This paper presents a methodology to estimate the regional probability of slope failure at the critical scale using local averaging theory with data provided by two DEMs.

The proposed methodology was illustrated using a test region of size 31 km × 48 km located in the Alps. Because of the test region's relatively large size, it is not surprising that the regional probability of slope failures at the assumed critical size of 10 m were relatively high (81%). At a slope scale of T_{crit} = 10 m it makes sense that at least one 10 by 10 m slope will fail in a region of size 31 km × 48 km with high probability.

If a community or organization wishes to incorporate landslide hazard analyses into their landslide preparation strategies, it might be prudent to divide large regions, such as the one considered earlier, into multiple subregions. For instance, the case study here suggests an 81% chance that at least one slope in the region examined in the Alps will fail, but whether or not the slope failure(s) will affect any of the communities in the region (e.g., Chamonix) is not provided by the model. It may make more sense to restrict attention to smaller regions surrounding communities. In addition, by breaking the analysis down into several smaller units, it becomes possible to pinpoint the most hazardous regions. In general, however, the size of the region selected should depend on the use to which the hazard assessment is put. Decisions regarding community-level planning will require smaller regions than those used at a national level.

The proposed hazard assessment model can be implemented for any study region, provided that the elevation profile within that region is approximately normally distributed and has been mapped by two DEMs at different resolutions. If the elevation profile is not approximately normally distributed, the methodology would need to employ a different final maximum slope distribution (i.e., something other than Rayleigh). If only one DEM resolution is available, the elevation point scale correlation length may have to be estimated using the single elevation dataset and some judgement about how the correlation length between the DEM local averages relates to the point scale correlation length.

The authors note that the probability of slope failure depends not only on slope angle but is also dependent on the slope height, which is a parameter not explicitly considered in this regional landslide hazard model. Clearly, the overall length and thus height of a slope affects its failure probability, and only the slope angle has been explicitly considered to be random in this study. Nevertheless, slope angle is generally the more important parameter and so if a reasonable "median" slope height is assumed in the preceding risk assessment framework, as was done in this study, the regional risks should be representative, at least relative to other regions.

Whether the critical scale slope failures will actually result in human hazard is another issue needing further study. However, the proposed methodology also provides a means to estimate slope failure probabilities at larger, more serious, scales. For example, the probability of regional slope failures at a slope scale of T_2 = 73 m was found to be about 64%, while at a slope scale of about T_1 = 773 m, the probability of regional slope failure decreases to 20%. These scale-dependent probabilities can be used in a more formal regional risk assessment if slope failure consequences are established.

Acknowledgements

The authors would like to thank the Natural Sciences and Engineering Research Council of Canada, under grant No. IPS1-363060, the International Centre for Geohazards, and the Norwegian Geotechnical Institute for their essential support of this research.

References

Chang, K., and Tsai, B. 1991. The effect of DEM resolution on slope and aspect mapping. Cartography and Geographic Information Science, **18**(1): 69–77. doi:10.1559/152304091783805626.

Chow, T.E., and Hodgson, M.E. 2009. Effects of lidar post-spacing and DEM

resolution to mean slope estimation. International Journal of Geographical Information Science, **23**(10): 1277–1295. doi:10.1080/13658810802344127.

Claessens, L., Heuvelink, G.B.M., Schoorl, J.M., and Veldkamp, A. 2005. DEM resolution effects on shallow landslide hazard and soil redistribution modelling. Earth Surface Processes and Landforms, **30**(4): 461–477. doi:10.1002/esp.1155.

Deng, Y., Wilson, J.P., and Bauer, B.O. 2007. DEM resolution dependencies of terrain attributes across a landscape. International Journal of Geographical Information Science, **21**(2): 187–213. doi:10.1080/13658810600894364.

Fenton, G.A., and Griffiths, D.V. 2008. Risk assessment in geotechnical engineering. John Wiley & Sons, New York.

Fenton, G.A., and Vanmarcke, E.H. 1990. Simulation of random fields via Local Average Subdivision. Journal of Engineering Mechanics, **116**(8): 1733–1749. doi:10.1061/(ASCE)0733-9399(1990)116:8(1733).

Gesch, D., and Greenlee, S. 1997. GTOPO30 documentation. Available from www1.gsi.go.jp/geowww/globalmap-gsi/gtopo30/README.html.

Griffiths, D.V., and Fenton, G.A. 2000. Influence of soil strength spatial variability on the stability of an undrained clay slope by finite elements. *In* Slope Stability 2000. Geotechnical Special Publication No. 101. ASCE, New York. pp. 184-193. doi:10.1061/40512(289)14.

Griffiths, D.V., and Fenton, G.A. 2004. Probabilistic slope stability analysis by finite elements. Journal of Geotechnical and Geoenvironmental Engineering, **130**(5): 507–518. doi:10.1061/(ASCE)1090-0241(2004)130:5(507).

Griffiths, D.V., Huang, J., and Fenton, G.A. 2009. Influence of spatial variability on slope reliability using 2-d random fields. Journal of Geotechnical and Geoenvironmental Engineering, **135**(10): 1367–1378. doi:10.1061/(ASCE)GT.1943-5606.0000099.

Jaedicke, C., Sverdrup-Thygeson, K., Vangelsten, B.V., Nadim, F., and Kalsnes, B. 2010. Work Project 2.4: Identification of landslide hazard and risk hotspots in Europe, Deliverable 2.10, SafeLand - Living with landslide risk in Europe. EU FP7 Research Project No. 226479.

Jones, K.H. 1998. A comparison of algorithms used to compute hill slope as a property of the DEM. Computers & Geosciences, **24**(4): 315–323. doi:10.1016/S0098-3004(98)00032-6.

JPL. 2009. SRTM homepage. Available from www2.jpl.nasa.gov/srtm.

McLean, A. 2011. Landslide risk assessment using digital elevation models. Master's thesis, Dalhousie University, Department of Engineering Mathematics, Halifax, N.S.

Nadim, F., Kjekstad, O., Peduzzi, P., Herold, C., and Jaedicke, C. 2006. Global landslide and avalanche hotspots. Landslides, **3**(2): 159–173. doi:10.1007/s10346-006-0036-1.

NIMA. 2000. Department of Defense World Geodetic System 1984: Its definition and relationship with local geodetic systems. National Imagery and Mapping Agency (NIMA). Available from: http://earth-info.nga.mil/GandG/publications/tr8350.2/wgs84fin.pdf. St. Louis, Mo.

Peitgen, H.-O., and Saupe, D. (*Editors*). 1988. The science of fractal images. Springer-Verlag, New York.

Raaflaub, L.D., and Collins, M.J. 2006. The effect of error in gridded digital elevation models on the estimation of topographic parameters. Environmental Modelling and Software, **21**(5): 710–732. doi:10.1016/j.envsoft.2005.02.003.

Smith, M.J., Goodchild, M.F., and Longley, P.A. 2007. Geospatial analysis: a comprehensive guide to principles, techniques and software tools. Matador, Leicester, UK.

United Nations Disaster Relief Coordinator (UNDRO) 1979. Natural disasters and vulnerability analysis. Report of the Expert Meeting Group, Geneva, Switzerland.

Vanmarcke, E.H. 1984. Random fields: analysis and synthesis. The MIT Press, Cambridge, Mass.

Zhang, X., Drake, N.A., Wainwright, J., and Mullian, M. 1999. Comparison of slope estimates from low resolution DEMs: Scaling issues and a fractal method for their solution. Earth Surface Processes and Landforms, **24**(9): 763–779. doi:10.1002/(SICI)1096-9837(199908)24:9<763::AID-ESP9>3.3.CO;2-A.

List of symbols

- A_t total area of the region under analysis
- Δd slope increment in degrees
- d_i ith slope angle in degrees = $i\Delta d$
- F_1 event that a single randomly selected slope fails
- $F_s(s)$ cumulative Rayleigh distribution function. S may be subscripted by 1 when referring to the first DEM (GTOPO) or by 2 when referring to the second DEM (SRTM)
- L_1, L_2 latitudinal coordinates of the edges of a DEM cell
- n_i number of slopes having slope angle s_i in the region
- n_s number of soil types considered in the analysis
- n_t number of slopes in the region
- N_{n_i} random number of slopes that fail out of those slopes having slope angle within the range s_i
- p_1 proportion of the region having the first soil type (fine-grained)
- p_2 proportion of the region having the second soil type (gravely)
- p_f probability of one or more slopes failing in the region
- p_{f_1} probability of one or more slopes failing in the region at the first DEM scale (GTOPO)
- p_{f_2} probability of one or more slopes failing in the region at the second DEM scale (SRTM)
- p_k proportion of the region having the kth soil type
- q_i probability of nonfailure of a slope having slope angle within the range s_i
- r_{1i} failure probability of the first soil type at the ith slope angle
- r_{2i} failure probability of the second soil type at the ith slope angle
- r_E radius of the Earth
- r_{ki} failure probability of the kth soil type at the ith slope angle
- S random slope angle
- S_T random slope angle perceived at averaging scale T. T may be subscripted by x or y to refer to the directional slopes, by 1 for the first (GTOPO) or 2 for the second (SRTM) DEM, by "m" to refer to the maximum slope, or by "m1" or "m2" for the maximum slopes in the first and second DEM, respectively.
- s slope angle (m/m)
- s_i ith slope angle range (m/m)
- s_{i-} lower bound on the slope angle range s_i (m/m)
- s_{i+} upper bound on the slope angle range s_i (m/m)
- s_{max} maximum slope angle considered (m/m)
- s_{min} minimum slope angle considered (m/m)
- T equivalent square dimension of an averaging cell. T may be subscripted by 1 to refer to the equivalent square cell dimension of the first DEM (GTOPO), by 2 for the second DEM (SRTM), or by *crit* for the critical scale
- T_x actual x-dimension of an averaging cell
- T_y actual y-dimension of an averaging cell
- x, y coordinates of a point in the region under consideration
- x_T, y_T coordinates of the center of a local average cell in the region
- $Z(x, y)$ true point surface elevation at the surface location (x, y)
- $Z_T(x_T, y_T)$ locally averaged surface elevation over a cell centered at (x_T, y_T)
- Δ_{lat} difference between two latitudinal points on the Earth's surface
- Δ_{long} difference between two longitudinal points on the Earth's surface
- Φ standard normal cumulative distribution function
- γ_Z variance function giving variance reduction due to averaging the elevation over some domain
- μ_{Z_T} mean of the local averaged surface elevations. T is subscripted by either 1 or 2 for the first (GTOPO) or second (SRTM) DEMs, respectively
- ρ_Z correlation coefficient between surface elevations at two points in the region
- ρ_{Z_T} correlation coefficient between two local averages of surface elevations
- σ_{S_T} standard deviation of the slopes as seen after locally averaging over cells of dimension $T \times T$. T may be subscripted by x for the x-direction slopes, by 1 for the first DEM scale (GTOPO), by 2 for the second DEM scale (SRTM), by *crit* for the critical scale, by 1x, 1y, 2x, 2y for the directional slopes in the first and second DEMs, or by m1 and m2 for the maximum slopes in the first and second DEMs, respectively
- σ_Z point scale standard deviation of the elevation Z
- σ_{Z_T} standard deviation of the locally averaged elevations Z_T. T may be subscripted by 1 for the first DEM scale (GTOPO), by 2 for the second DEM scale (SRTM)
- τ absolute distance between two points, or between the centers of two local averages
- τ_x absolute distance between two points in the x-direction
- τ_y absolute distance between two points in the y-direction
- θ_Z isotropic point scale correlation length of the elevation field
- θ_{Z_x} x-direction correlation length of the elevation field
- θ_{Z_y} y-direction correlation length of the elevation field